Sustainable Energy Technologies and Assessments 52 (2022) 102036

Contents lists available at ScienceDirect

Sustainable Energy Technologies and Assessments

journal homepage: www.elsevier.com/locate/seta

A solar thermal sorption-enhanced steam methane reforming (SE-SMR) approach and its performance assessment

Andrey Gunawan [a], Abhishek K. Singh [b,*]

[a] George W. Woodruff School of Mechanical Engineering, Georgia Institute of Technology, Atlanta, GA 30332 USA
[b] Faculty of Engineering Technology, Department of Thermal and Fluid Engineering, University of Twente, Postbus 217, 7500 AE Enschede, the Netherlands

ARTICLE INFO

Keywords:
Solar
SE-SMR
Solar-to-fuel conversion
Thermochemical
Hydrogen
Efficiency

ABSTRACT

This paper proposes an integration of concentrating solar power (CSP) with a sorption-enhanced steam methane reforming (SE-SMR) process and assesses its overall solar-to-fuel conversion performance. A thermodynamic treatment of the SE-SMR process for H_2 production is presented and evaluated in an innovative two reactors system configuration using CSP as a heat input. Four metal carbonate/metal oxide pairs are considered, and the equilibrium thermodynamics reveals that $CaCO_3$/CaO pair is the most suitable candidate for this process. Additionally, a reactor-scale thermodynamic model is developed to determine the optimum operating conditions for the process. For the carbonation step, temperatures between 700 and 900 K and steam-to-methane ratio $\geq$4 are found to be the most favorable. Furthermore, an advanced process model, which utilizes operating conditions determined from the reactor-scale model, is developed to evaluate the process efficiency. The model predicts that the proposed process can achieve a solar-to-fuel efficiency ~41% for calcination temperature of 1500 K and carbonation temperature of 800 K, without considering any solid heat recovery. An additional 2.5% increase in the process efficiency is feasible with the consideration of the solid heat recovery. This study shows the thermodynamic feasibility of integrating the SE-SMR process with CSP technologies.

1. Introduction

Hydrogen (H_2) has been considered as the next generation energy carrier for the development of a clean, sustainable energy infrastructure [1–3]. Currently, most H_2 in the world is produced using the steam methane reforming (SMR) process, which comprises numerous steps and harsh operating conditions [3]. In order to improve the SMR process, various researchers have investigated the sorption-enhanced steam methane reforming (SE-SMR) process, which is an SMR process that incorporates in situ carbon dioxide (CO_2) capture [4–7]. In the SE-SMR process, a CO_2 acceptor is deployed together in the reactor with a reforming catalyst to take the CO_2 out from the product gas stream of the reaction [4]. This direct removal process of the CO_2 follows the Le'Chatelier's principle, shifting the equilibrium towards the product side, which is in turn favorable in increasing the H_2 production [8]. Metal oxide, which is the CO_2 acceptor, can be regenerated from metal carbonate using thermal decomposition. Several researchers have used CaO-based sorbents, although recently Li- and Na-based metal oxides were also reported as candidate materials for CO_2 removal [5,7]. Both the SMR and SE-SMR processes require high temperature (>600 °C) to carry out the endothermic reaction. Concentrating solar power (CSP) can provide the required process heat [9,10], and therefore it can serve as a clean and renewable energy source alternative for these processes.

CSP integration with the SMR (CSP-SMR) process has been an active topic of several studies. There are review and short-review articles [11–13] that compiled and discuss creditable progress made to improve the CSP-SMR process recently. Some notable examples are Rubin and Karni [14], who were among the first to experimentally investigate the efficiency of solar thermal SMR reactor. They designed a new solar volumetric reactor, for CO_2 reforming of methane (CH_4), which they tested on top of a solar tower. A CH_4 to CO_2 ratio of 1.2 and a maximum absorber temperature of 1450 K were maintained throughout the experiments, and they were able to achieve solar-to-fuel efficiency ~ 30%. The study focused more on the reactor design and performance, and heat recovery option from the product gases were not considered. Another study in 2014 by Gokon et al. [15] reported a solar-to-fuel efficiency up to 29% using a lab-scale SMR reactor that was integrated with molten carbonate salts-based thermal energy storage system. An electric furnace was used to simulate the CSP heat input throughout the day. With this integrated storage system configuration, the authors concluded that the

* Corresponding author.
E-mail address: a.k.singh@utwente.nl (A.K. Singh).

https://doi.org/10.1016/j.seta.2022.102036
Received 9 January 2021; Received in revised form 18 June 2021; Accepted 25 January 2022
Available online 8 February 2022

impact of intermittency of solar radiation could be mitigated. Although it provided heat recovery possibility from the reactor, the fraction of recovered heat was limited because the solids, namely the catalyst and the storage medium, remain in the reactor. Moreover, in 2019 Pashchenko [16] investigated SMR process to understand the effect of catalyst particle shape on the pressure drop and CH_4 conversion. A cylindrical packed bed of particles filled with Ni-αAl_2O_3 catalyst were used for the experiments. The study showed that CH_4 conversion increases with the increase in the geometrical surface area of the packed bed particles. The packed bed filled with simple cylindrical shape particles developed much higher pressure drops across the bed as compared to the packed bed filled with 7-holes cylinders. In another study, Giaconia et al. [17] reported the integration of CSP with a membrane-based SMR reactor, which allows for constant removal of H_2 from the catalytic section, thereby pushing the reaction towards the product formation. A more recent study by Bulfin et al. [18] compared two solar thermochemical reforming routes; redox reforming and catalytic reforming. Thermodynamic analysis of both processes were performed and compared for the CH_4 conversion extents, syngas composition, and energy conversion efficiencies. The study found that redox reforming can provide a higher quality syngas than the catalytic reforming.

Some researchers also provided insight into the CSP-SMR process numerically. Ngoh et al. [19] designed, optimized and simulated a large hybrid CSP-powered H_2 production system. The SMR process was powered by an 8 MW photovoltaic plant that was simulated under Sudanese Sahelian conditions of Sudan type. The simulation was performed using the generalized reduced gradient algorithm to estimate the theoretical production rate of H_2, which the authors reported to be 1,843.2 kg day^{-1}. Embarking from their previous work, Said et al. [20] investigated the thermal effects of a tube-and-shell, molten salt-heated packed bed membrane reformer (Ni/Al_2O_3 catalyst, 5 um supported Pd film membrane) using a detailed computational fluid dynamics (CFD) model in a non-isothermal conditions that were relevant to parabolic trough collector system. The authors also presented a techno-economic analysis for this CSP-SMR system. This newer study, specifically, looked into the effects of the molten salt and reforming feed flow rates on temperature gradients and H_2 distribution, evaluating the reformer performance in terms of conversion, H_2 recovery and selectivity to carbon monoxide (CO). The authors reported that, in an optimum case, CH_4 conversion of 0.99 and H_2 recovery of 87% were achieved with molten salt feed temperature of 600 °C and reforming feed space velocity of 5,000 h^{-1}, which corresponds to a power density of 1.9 kWL^{-1} and a fuel heating value upgrade of 40%. Wang et al. [21] numerically studied the feasibility of integrating SMR with mid- or low-temperature CSP technologies. They reported that a net solar-to-fuel efficiency can reach as high as 38.25% at temperature $>$ 400 °C, after taking real vacuum pump and compressor efficiencies into account. More recently, Pashchenko [22] performed a thermodynamic equilibrium analysis of the SMR to determine the optimal operating conditions for the highest steam-to-methane conversion. The analysis depicted no carbon formation at temperatures higher than 1100 K for steam-to-methane ratio >1. While these studies have focused on the SMR processes, we found that the integration of CSP with the more efficient SE-SMR process has never been investigated before.

Indeed, the H_2 production technology via SE-SMR process (without CSP integration) has also been well-studied. Its latest research can be found in a number of review articles [5–7]. However, not all of the recent studies were covered. In 2019, Di Felice et al. [23] investigated a mayenite supported 30 wt% CaO-based sorbent powders mixed with a commercial 5.2 wt% Ni catalyst for SE-SMR process during an EU-FP7 ASCENT project. The authors reported that the new combined sorbent-catalysts materials (CSCM) had initial CO_2 sorption capacity of $\sim$ 16% (*i.e.,* $16g_{CO_2}/100g_{CSCM}$), which progressively declined and stabilized at 10% after 90 (out of 100) consecutive sorption-regeneration cycles. The authors associated the gradual 37.5% decrease in sorption capacity to CaO depletion in the sorbent by chemical interactions with the Ni catalyst, which led to formation of additional mayenite and Ni solid solution accumulation. Di Giuliano et al. [24] summarized the whole experimental results over 4 years working period in the abovementioned EU-FP7 ASCENT project. Among the significant findings, the CSCM with the lowest free CaO content and the highest Ni load, CaO15Ni(N)10, was reported to be fully active and stable for$>$200 SE-SMR/mild-regeneration (in N_2 at 850 °C) cycles in a packed-bed microreactor at 650 °C and 1 atm. A 5% decrease in sorption capacity was observed from 10.4% ($10.4g_{CO_2}/100g_{CSCM}$) of the fresh sample to 9.9%, which was still higher than the minimum required value of 8.5% of the ASCENT project. Additionally, Acha et al. [25] developed a cheaper Ni-based catalyst to produce high purity H_2 via SE-SMR of bio oils. They tested seven Ni-based catalysts that were prepared using conventional Al_2O_3 support and non-conventional olivine sand, with Co and Pd additions, arctic dolomite and the cheaper raw dolomite. They found that it was possible to obtain 99.89% pure H_2 using Ni-based catalyst with the cheaper olivine support, however, the more expensive Arctic Dolomite showed much better sorption performance than the cheaper raw dolomite because it has higher pore volume. While no significant catalytic performance differences were detected with the addition of the Co or Pd, the sorption capacity of each catalyst strongly decreased after the first SE-SMR cycle with bio-oil compounds performed with Artic Dolomite at 575 °C and 1 atm. More recently, Chen et al. [26] experimentally showed that a fuel cell grade H_2 (with 98.8% purity and $<$0.1 ppm CO) could be obtained from an optimized SE-SMR process performed at $\sim$550 °C, 2600 $cm^3\ g^{-1}h^{-1}$ space velocity, and a steam-to-carbon ratio (S/C = 4). They utilized a homogenous dispersion of 20 wt% Ni/Al_2O_3 and CaO sorbent composite as the reforming catalyst, which the authors claimed to be prepared by a simple physical mixing and granulation to a columnar shape, to obtain a product stream with $>$95% H_2 content and a CH_4 conversion of 0.90.

Similarly, computational strategies have also been used more recently to provide insight into the SE-SMR process. Phuakpunk et al. [27] used a CFD approach with 2-D transient models using the Euler-Euler approach and kinetic theory of granular flows, combined with the decarbonation kinetics of dolomite, to design a conceptual pilot-scale circulating fluidized bed reactor system for SE-SMR processes. They showed that it was feasible to continuously produce high purity H_2 via SE-SMR process using a properly designed double-stage bubbling bed regenerator system (with 1.2 m width, 0.8 m bed height, a flux of returning solids of 200 kg $m^{-2}s^{-1}$, and a catalyst-to-sorbent ratio of 2.54) when it was operated with a carrier gas inlet velocity of 0.2 m s^{-1} and preheating of the solids at 950 °C. In addition, Nkulikiyinka et al. [28] utilized machine learning models to assist scaling up a SE-SMR process. They developed and compared the artificial neural networks and random forest (RF) models, to predict and estimate variables that would otherwise be difficult to measure experimentally. Temperature, pressure, S/C, and sorbent-to-carbon ratio were used as inputs. And the evaluated outputs were operating parameters, which include reactor gas concentrations, reformer CH_4 conversion, and overall process H_2 purity at specified conditions. The authors claimed that the machine learning approach had advantages over thermodynamic simulations, especially in obtaining real time information that was dependent on actual process conditions. Even though the results had not been validated with experiments, the authors concluded that both models were very accurate, although the RF model was more precise in the predictions with higher R_2 values and lower mean absoluter error. Yan et al. [29] evaluated and compared six different SE-SMR configurations via a thermodynamic analysis using Aspen Plus with a detailed heat exchanger modeling to recover waste heat from each process according to the second law of thermodynamics. They found that a SE-SMR with a Pressure Swing Adsorption (PSA) and Chemical-Looping Combustion units could realize nearly 100% carbon capture with the highest net operating efficiency of 75.5% while operating at a reformer temperature of 600 °C, a reformer pressure of 25 bar, and a S/C = 5. On the other hand, a SE-SMR with a

PSA and an indirect H_2-fired calciner units, where a proportion of H_2 was recycled to provide heat for the calcination process, was able to achieve 94.2% carbon capture efficiency with a trade-off in cold gas efficiency of 51.3%. Most recently, Neni et al. [30] performed CFD simulations using a fixed-bed reactor, by considering an effective medium thermal conductivity for the case of thermal equilibrium between the solids (70% Ni/Al_2O_3 catalyst and 30% CaO sorbent) and gaseous phase, to study the effect of CO_2 capture onto a CaO sorbent on the performance of the SE-SMR process. They reported that the maximum H_2 outlet molar fraction (dry basis) was 0.8 with the CO_2 sorption, which dropped to 0.42 once the sorbent reached its maximum conversion degree.

In all of the aforementioned studies, the SE-SMR and regeneration steps are carried out in the same reactor, which makes it a batch process. Herein we argue that by using a two-reactor approach, the SE-SMR process can be used to continuously produce H_2. In this latter approach, either (i) inlet reactant gas supplies are switched between reactors carrying out the SE-SMR and the regeneration steps, or (ii) solid products from both reactions are moved in between the reactors continuously. The first process can be implemented by controlling the reactant gas supply using valve mechanisms. In the second process, transfer of high-temperature solids will require appropriate piping materials and a mechanism for moving high-temperature solids between reactors. Nonetheless, the second process can be advantageous for solid heat recovery, which can increase the overall process efficiency [31]. Accordingly, we only consider the second process in the current analysis, which is one of the innovative elements of the present study. All in all, this study represents the integration of CSP, which to the best of our knowledge has never been applied to the SE-SMR processes.

2. Methodology

Herein, the analysis focuses on the utilization of a two-step calcination-carbonation process (Fig. 1), which primarily relies on a solid–gas reaction for H_2 production and CO_2 capture. Metal oxide reacts with CH_4 and steam and produces metal carbonate in solid phase and H_2 in gas phase in the carbonation process:

$$MO + CH_4 + 2H_2O \rightarrow MCO_3 + 4H_2,\ \Delta h < 0 \text{ (exothermic reaction)} \quad (1)$$

In the calcination process, the metal oxide is recovered from the metal carbonate by thermal decomposition:

$$MCO_3 \rightarrow MO + CO_2,\ \Delta h > 0 \text{ (endothermic reaction)} \quad (2)$$

The produced CO_2 can then be sequestered or used to produce various useful chemicals [32,33]. Furthermore, the integration of CSP with the endothermic calcination step is considered. Here, a selection of four metal oxide/metal carbonate pairs ($SrO/SrCO_3$, $MgO/MgCO_3$, $BaO/BaCO_3$, and $CaO/CaCO_3$) are investigated by comparing the equilibrium thermodynamics of each pair. After the optimal material is selected, a viability analysis using a reactor-scale thermodynamic model is carried out to find the optimal working conditions of the calcination/carbonation reactions. The effect of steam-to-methane ratio over the carbonation reaction is also determined using this model. The reactor-scale model is further developed by integrating CSP with the process. This final model is utilized to predict the overall energy efficiency and the impacts of gas/solid phase heat recovery, steam-to-methane ratio, and concentration ratio over the process efficiency.

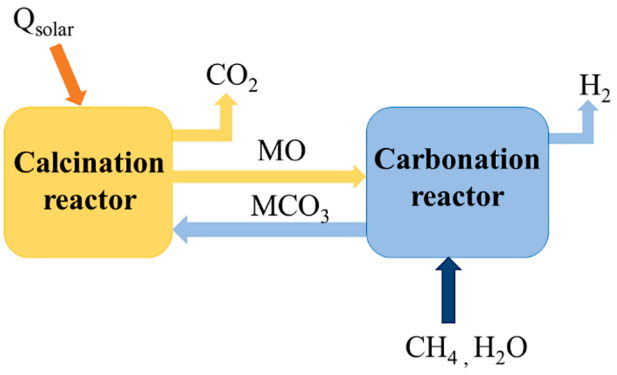

Fig. 1. Schematic of a two-step calcination-carbonation process in a solar thermal sorption-enhanced steam methane reforming (SE-SMR) approach.

2.1. Equilibrium thermodynamics

The equilibrium temperatures of carbonation/calcination reactions for the four different metal carbonate/metal oxide pairs are compared by using the change in Gibb's free energy (ΔG) of the reactions. Fig. 2a shows the variation of ΔG with temperature for the considered calcination reactions, namely Eq. (2). For a range of temperature where $\Delta G \leq 0$, the reaction is spontaneous. Therefore, $MgCO_3$ calcination is thermodynamically feasible at lower temperatures ($T \geq 750$ K) and for $BaCO_3$ at higher temperatures ($T \geq 1800$ K). For $CaCO_3$ and $SrCO_3$, the feasible calcination temperatures are ≥ 1250 K and 1400 K, respectively.

Fig. 2b shows that for the carbonation reaction, Eq. (1), all the considered species except MgO show thermodynamic feasibility in the whole temperature range between 300 and 2000 K. In contrast, MgO carbonation reaction is thermodynamically favorable at temperatures higher than 1300 K. The higher operating temperatures, however, lead to higher losses, containment material restrictions, and ultimately

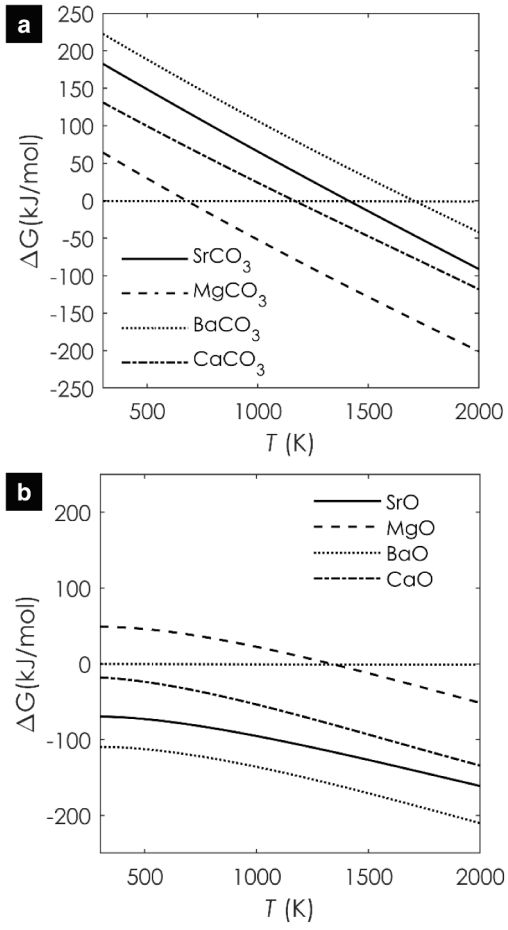

Fig. 2. (a) Variation of the change of Gibbs free energy (ΔG) with temperature (T) for four metal carbonate calcination reactions ($MO + CH_4 + 2H_2O \rightarrow MCO_3 + 4H_2$); (b) Variation of ΔG with T for the four metal oxide carbonation reactions ($MCO_3 \rightarrow MO + CO_2$).

higher costs. Considering that the calcination reaction of $BaCO_3$ also requires higher temperatures $\geq$ 1800 K, Ca- and Sr-based pairs become the more reasonable choice. Additionally, because the $CaCO_3$ calcination reaction is thermodynamically feasible at lower temperatures than $SrCO_3$, the Ca-based calcination-carbonation process is considered in the subsequent analyses, because of its lower operating temperatures and potentially lower costs.

2.2. Reactor-scale thermodynamic model

A reactor-scale thermodynamic model [34] is used to identify the optimal process conditions for the calcination-carbonation reactions. This model simulates a solid–gas equilibrium reaction in a reactor in which reactant gases are injected in the reactor containing solid reactant, and the ensuing product gases are constantly removed from the reactor while solid products remain in the reactor. The ideal gas behavior for the gaseous species and incompressibility for the solid phase is considered. For the reaction system, the following nine species are considered in the thermodynamic equilibrium model: H_2, O_2, CO, CO_2, CH_4, C, $CaCO_3$, $Ca(OH)_2$, and CaO. The equilibrium compositions are calculated using the constrained minimization (arg min) of the reaction system's Gibbs free energy, which is calculated by assuming two separate phases (mixture of ideal gases and perfectly mixed incompressible solids) in close contact. That is [34],

$$y_{i,\mathrm{gas/solid},eq}\left(\boldsymbol{n}_{\mathrm{gas}},\boldsymbol{n}_{\mathrm{solid}},T,p\right)=\underset{\mathbf{n}_{\mathrm{gas}},\mathbf{n}_{\mathrm{solid}}}{\mathrm{argmin}}G(\boldsymbol{n}_{\mathrm{gas}},\boldsymbol{n}_{\mathrm{solid}},T,p) \tag{3}$$

where

$$G=\sum_{i=1}^{n}G_{\mathrm{i,gas}}+\sum_{i=1}^{m}G_{\mathrm{i,solid}} \tag{4}$$

and $G_{\mathrm{i,gas}}$ and $G_{\mathrm{i,solid}}$ are defined by Singh et al. [34]

$$G_{i,gas}=n_i g_i^{-O}+n_i RTln\left(y_i P/P_{ref}\right) \tag{5}$$

$$G_{\mathrm{i,solid}}=n_i\overline{g}_i^{0}+n_i RT\ln y_i \tag{6}$$

where n_{i} is the number of moles of a species (kmol), $\overline{g}_i^{0}$ the reference Gibbs function of species i that is being evaluated (kJ kmol^{-1}), R the universal gas constant (kJ kmol^{-1} K^{-1}), T the reaction temperature (K), y_{i} the species i mole fraction, P the total system pressure (N m^{-2}), and P_{ref} the reference pressure (N m^{-2}). The number of moles of the considered species are conserved to keep the balance of elements intact during the process. The thermodynamic properties are extracted from the FactSage web database [35].

2.3. Process model

The model developed in the previous section is enhanced by integrating CSP with the SE-SMR process. The optimized process conditions and reaction output determined by the reactor-scale model is used for calculating the overall process efficiency. Fig. 3 shows the schematic of the $CaCO_3$ calcination and CaO carbonation processes carried out in separate reactors with required heat exchangers for the recovery of heat. The exchange of solid products between carbonation and calcination reactors are depicted in the schematic with labels of various inlet/outlet temperatures. The process layout also includes a unit for the separation of CH_4, CO, and CO_2 from the carbonation reaction exhaust stream.

Calcination is an endothermic process, and herein its energy requirement will be fulfilled by process heat from the CSP $\left(\dot{q}_{\mathrm{solar}}\right)$. The heat exchangers HX1 and HX2 are used to preheat the incoming gaseous reactants, CH_4 and H_2O, using the high-temperature exhaust gases from the carbonation and calcination processes, respectively. The $\dot{q}_{\mathrm{solar}}$ provides the necessary heat for the calcination reaction, increasing the temperature of $CaCO_3$ from T_{carb} to T_{cal}. Some unreacted CH_4 or unwanted product gases, such as CO and CO_2 may be present in carbonation outlet gases. A membrane separation process can be used to extract these gases, and the required separation energy $\left(\dot{q}_{\mathrm{sep,total}}\right)$ is also included in this analysis. Due to the complete solid–gas mixing assumption, solids and gases are expected to have the same temperature at the end of the processes.

CaO (s) formed during the calcination reaction at T_{cal} is moved to the carbonation reactor. The solid and gaseous reactants of the carbonation reaction can be heated by utilizing the exothermic heat of the reaction. To keep the isothermal operation of this reaction, excess heat needs to be vented to the atmosphere. Similarly, the carbonation reaction product ($CaCO_3$) is moved to the calcination reactor after the completion of the process. This transportation is assumed to be having negligible heat loss.

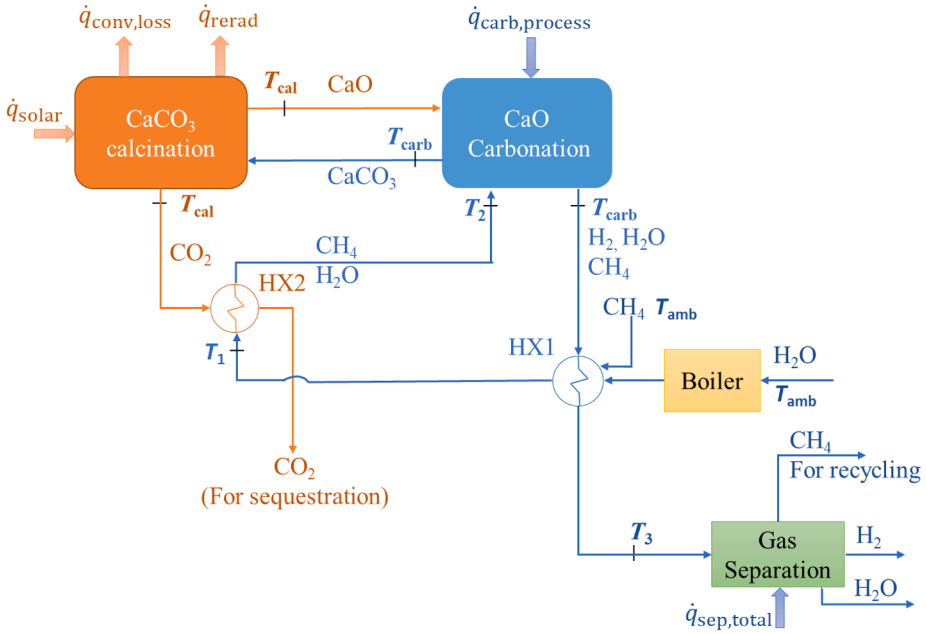

Fig. 3. Energy and mass flow diagram of the proposed solar thermal sorption-enhanced steam methane reforming (SE-SMR) process with two reactors.

We also assume that the pressure throughout the process is atmospheric. The energy balance of the overall system can be represented in the following form:

$$\dot{q}_{\text{solar}} = \dot{q}_{\text{cal,rxn}} + \dot{q}_{\text{CaCO}_3,T_{\text{carb}}\rightarrow T_{\text{cal}}} + \dot{q}_{\text{conv,loss}} + \dot{q}_{\text{rerad}} + \dot{q}_{\text{carb,process}} \tag{7}$$

where $\dot{q}_{\text{cal,rxn}}$ is the energy required for the calcination reaction inside the calcination reactor, and $\dot{q}_{\text{CaCO}_3,T_{\text{carb}}\rightarrow T_{\text{cal}}}$ the energy required to heat $CaCO_3$ from the carbonation temperature T_{carb} to the calcination temperature T_{cal}. These two variables are not shown in Fig. 3, because the energy flows happen inside the calcination reactor (control volume). $\dot{q}_{\text{conv,loss}}$ and $\dot{q}_{\text{rerad}}$ account for the convective and radiative heat losses from the reactor, which also functions as a solar receiver. The last variable in $\dot{q}_{\text{carb,process}}$ is the energy needed for the carbonation process:

$$\dot{q}_{\text{carb,process}} = \dot{q}_{\text{CH}_4+\text{H}_2\text{O},T_2\rightarrow T_{\text{carb}}} - \dot{q}_{\text{carb,rxn}} - \dot{q}_{\text{CaO},T_{\text{cal}}\rightarrow T_{\text{carb}}} \tag{8}$$

where $\dot{q}_{\text{CH}_4+\text{H}_2\text{O},T_2\rightarrow T_{\text{carb}}}$ is the required energy for preheating the reactant gases to the carbonation temperature T_{carb}, $\dot{q}_{\text{carb,rxn}}$ the energy released by the exothermic carbonation reaction, and $\dot{q}_{\text{CaO},T_{\text{cal}}\rightarrow T_{\text{carb}}}$ the energy available after cooling CaO from calcination temperature T_{cal} to the carbonation temperature T_{carb}. These three variables are also not shown in Fig. 3, because the energy flows happen inside the carbonation reactor (control volume). If $\dot{q}_{\text{CH}_4+\text{H}_2\text{O},T_2\rightarrow T_{\text{carb}}} \leq \dot{q}_{\text{carb,rxn}} + \dot{q}_{\text{CaO},T_{\text{cal}}\rightarrow T_{\text{carb}}}$, then $\dot{q}_{\text{carb,process}} = 0$.

Energy balance calculations are performed to find the outlet gas temperatures of the heat exchangers HX1 and HX2. For HX1, the amount of heat transfer can be written as

$$\dot{q}_{\text{HX1}} = \epsilon \bullet \min\left(\begin{array}{c} \dot{n}_{\text{CH4}}\left(h_{\text{CH}_4,T_1} - h_{\text{CH}_4,T_{\text{amb}}}\right) + \dot{n}_{\text{H}_2\text{O}}\left(h_{\text{H}_2\text{O},T_1} - h_{\text{H}_2\text{O},T_{\text{amb}}}\right) \\ \dot{n}_{\text{H}_2}\left(h_{\text{H}_2,T_3} - h_{\text{H}_2,T_{\text{carb}}}\right) + \dot{n}_{\text{H}_2\text{O}}\left(h_{\text{H}_2\text{O},T_3} - h_{\text{H}_2\text{O},T_{\text{carb}}}\right) + \dot{n}_{\text{CH}_4}\left(h_{\text{CH}_4,T_3} - h_{\text{CH}_4,T_{\text{carb}}}\right) + \dot{n}_{\text{CO}}\left(h_{\text{CO},T_3} - h_{\text{CO},T_{\text{carb}}}\right) \end{array}\right) \tag{9}$$

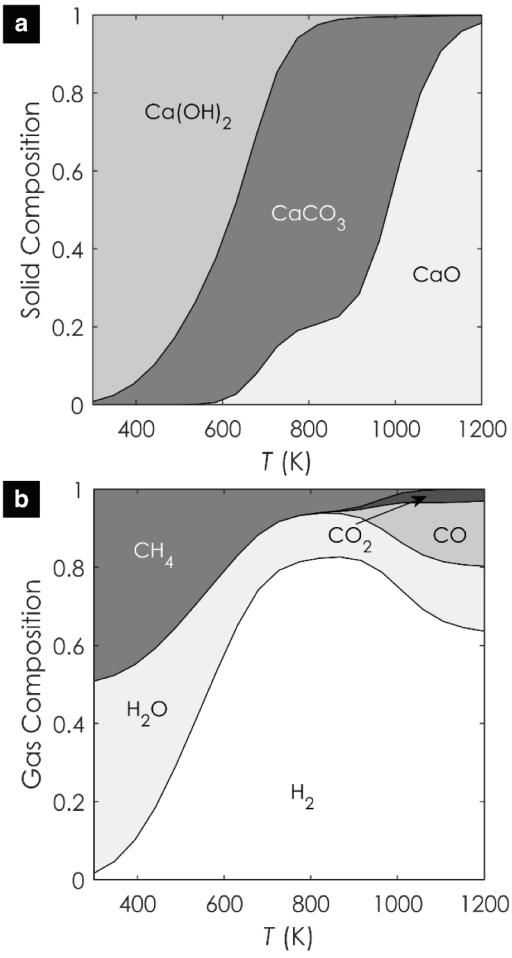

Fig. 4. (a) Variation of solid composition with temperature, and (b) variation of aggregate gaseous composition with temperature for CaO carbonation reaction considering stoichiometric amounts of the reactants.

where ϵ is the heat exchanger effectiveness, $\dot{n}$ molar flow rate (kmol s^{-1}), and h enthalpy (kJ mol^{-1}). The temperatures T_1 and T_3 are calculated by using:

$$\dot{q}_{\text{HX1}} = \dot{n}_{\text{CH4}}\left(h_{\text{CH}_4,T_1} - h_{\text{CH}_4,T_{\text{amb}}}\right) + \dot{n}_{\text{H}_2\text{O}}\left(h_{\text{H}_2\text{O},T_1} - h_{\text{H}_2\text{O},T_{\text{amb}}}\right) \tag{10}$$

and:

$$\begin{aligned}\dot{q}_{\text{HX1}} = {} & \dot{n}_{\text{H}_2}\left(h_{\text{H}_2,T_3} - h_{\text{H}_2,T_{\text{carb}}}\right) + \dot{n}_{\text{H}_2\text{O}}\left(h_{\text{H}_2\text{O},T_3} - h_{\text{H}_2\text{O},T_{\text{carb}}}\right) \\ & + \dot{n}_{\text{CH}_4}\left(h_{\text{CH}_4,T_3} - h_{\text{CH}_4,T_{\text{carb}}}\right) + \dot{n}_{\text{CO}}\left(h_{\text{CO},T_3} - h_{\text{CO},T_{\text{carb}}}\right)\end{aligned} \tag{11}$$

Similarly, $\dot{q}_{\text{HX2}}$, T_2, and T_4 for the second heat exchanger (HX2) are calculated using the same method.

With an assumption of an effective emissivity of 1, the absorption losses in the receiver can be neglected. Therefore, the re-emission to the ambient $\dot{q}_{\text{rerad}}$ are defined by Krenzke and Davidson [36]

$$\dot{q}_{\text{rerad}} = \frac{\sigma T_{red}^4}{C G_{inc}} \dot{q}_{\text{solar}} \tag{12}$$

where σ is the Stefan-Boltzmann constant, T_{red} the reduction temperature (K), C is the concentration ratio (-), and G_{inc} the direct normal irradiance (W m^{-2}). Additionally, the convective losses $\dot{q}_{\text{conv,loss}}$ are accounted as a fraction of the difference between the incident and re-emitted energies, which can be simply represented in the following form [37]:

$$\dot{q}_{\text{conv,loss}} = F(\dot{q}_{\text{solar}} - \dot{q}_{\text{rerad}}) \tag{13}$$

where F is the heat loss factor (-). Moreover, the minimal amount of energy for gas separation is given by [38]

$$E_{\text{sep,min,i}} = RT\ln\left(\frac{1}{y_i}\right) \tag{14}$$

Practically, the separation process involves other forms of works (*i.e.* mechanical or electrical) with a fixed conversion efficiency. Therefore, following our previous study, an efficiency (corresponding to the mechanical or electrical work related to the separation process) η_{w} of 10% is also considered in this analysis [38]:

$$\dot{q}_{\text{sep,total}} = \sum_i \dot{n} \frac{E_{\text{sep,min,i}}}{\eta_{\text{w,i}}} \tag{15}$$

Lastly, the solar-to-fuel efficiency is defined by

$$\eta = \frac{\dot{n}_{\text{H}_2} HHV_{\text{H}_2} - \dot{n}_{\text{CH}_4} HHV_{\text{CH}_4}}{\dot{q}_{\text{solar}} + \dot{q}_{\text{sep,total}}} \tag{16}$$

where the higher heating values (HHV) of H_2 (286 kJ mol^{-1}) and CH_4 (888.3 kJ mol^{-1}) are used.

3. Results and discussion

The reactor-scale model described in section 2.2 is utilized to find the yields of calcination and carbonation steps of the $CaCO_3$/CaO process. In the carbonation step, CaO reacts with CH_4 and steam at various temperatures between 300 and 1200 K and 1 bar pressure. The stoichiometric ratios of reactants are used in the analysis. An open system reactor operation in which product gases are continuously removed from the reactor but solids stay in the reactor is assumed in the analysis.

Fig. 4a shows the composition of solid products at various temperatures during the carbonation reaction. The majority of $CaCO_3$ formation occurs between a narrow temperature range of 700 to 900 K, which has also been observed in experimental investigations by Broda et al. [39]. The thermodynamic model predicted the formation of a higher fraction of $Ca(OH)_2$ and CaO at lower (T < 700 K) and higher (T > 900 K) temperatures, respectively. The gas phase composition of the carbonation reaction is shown in Fig. 4b. The H_2 production is higher between 700 and 900 K due to the higher extent of reaction completion. CH_4 cracking is incomplete at lower temperatures (T < 700 K), therefore most of the H_2 production is due to water splitting only. At higher temperatures (T > 900 K), CaO reaction with CO and CO_2 gases (produced from cracking of CH_4) is not favorable, therefore, exhaust gas in this temperature range contains considerable amounts of these carbonaceous gases. The model does not predict any carbon formation, which is also in line with experimental observations by Chanburanasiri et al. [40]. For the stochiometric ratios of CH_4 and steam, exhaust gases contain CH_4, CO, and CO_2 along with H_2 in the considered temperature range. Due to these unwanted gases, another purification step of the exhaust gases must be performed to obtain a pure steam of H_2, which consecutively decreases the overall process efficiency. To alleviate this issue, further analysis is performed in which steam-to-methane molar ratio is increased and its effect over the carbonation reaction is determined using the thermodynamic model.

Fig. 5a and b show the gas phase composition considering steam-to-methane molar ratios of 4 and 6, respectively. The higher steam amount in the system favors the formation of $CaCO_3$, which in turn decreases the formation of carbon-containing gases between 700 and 900 K. The effect of steam-to-methane molar ratio over $CaCO_3$ formation is shown in Fig. 5c. With the increase of steam-to-methane ratio, $CaCO_3$ formation also increases. To obtain a pure H_2 production, steam-to-methane molar ratio ≥ 4, and a temperature range of 700 to 900 K is recommended for this step of the process. For the calcination reaction, the variation of the molar ratio of the product species (solid and gas) and stochiometric moles of the same species with temperature is shown in Fig. 5d. At 1 bar pressure, the calcination reaction shows completion at temperatures close to 1500 K.

The favorable operating conditions determined using the reactor-scale model are utilized in the process model to calculate the solar-to-fuel efficiency η for various parameters. For this analysis, the reduction and oxidation reactions are assumed to be 1500 and 800 K, respectively. The effect of the steam-to-methane molar ratio over η is determined, and the impacts of C and ϵ over η are also investigated. Both heat exchangers shown in Fig. 3 are assumed to have the same ϵ. Although 1 kW CSP input $\dot{q}_{solar}$ is assumed for the current study, the outcomes can be scaled to any $\dot{q}_{solar}$ values. F of 0.2 from our previous study [41] is used to find the convection losses from the reactor, $\dot{q}_{conv,loss}$ (Eq. (13)).

First, a C that maximizes the η of the process is determined. The corresponding plot is shown in Fig. 6a. No heat recuperation in any form is assumed for this calculation. Although higher C increases the η, only

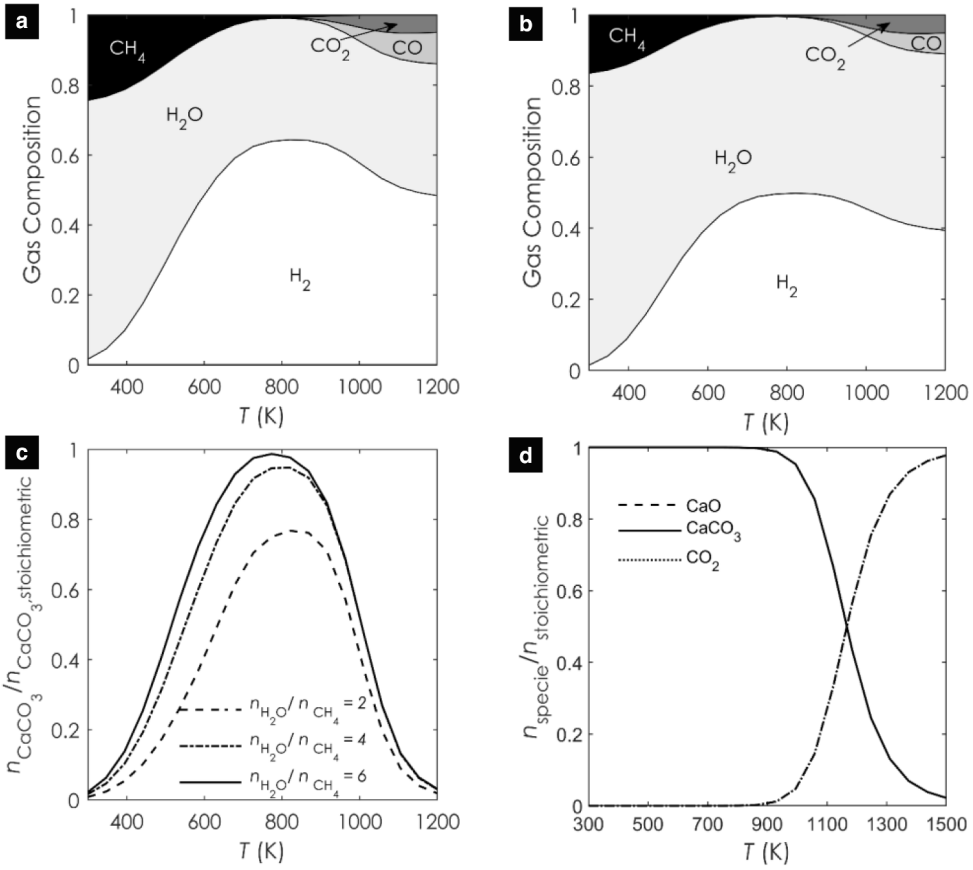

Fig. 5. (a) Variation of aggregate gaseous composition with temperature for CaO carbonation reaction considering steam-to-methane molar ratio of 4, and (b) steam-to-methane molar ratio of 6; (c) Variation of the molar ratio of produced and stoichiometric amounts of $CaCO_3$ with reaction temperatures for different steam-to-methane molar ratios; (d) Changes in the solid phase fractions with temperature for $CaCO_3$ calcination reaction considering stoichiometric amounts of the reactants.

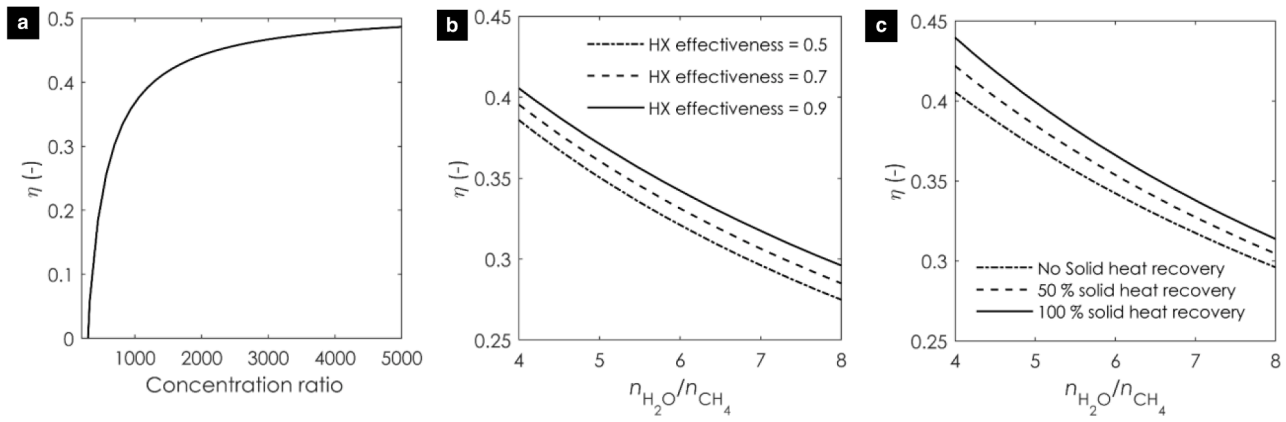

Fig. 6. (a) Variation of η with C, where heat recovery is neglected and the oxidation and reduction temperatures are 800 K and 1500 K, respectively); (b) Variation of η with steam-to-methane molar ratio, where ϵ is varied, and $C = 2000$ is used in the calculations; (c) Variation of η with steam-to-methane molar ratio, where the fraction of solid heat recovery is varied, $C = 2000$ and $\epsilon = 0.9$ are used in the calculations.

1% increase is predicted by the model for $C > 2000$. An increase in C comes with a higher cost. Therefore, $C = 2000$ is assumed for the following analysis. During the analysis, it is found that the carbonation process is self-sustaining ($\dot{q}_{carb,process} = 0$) and no external energy input is required for this reaction. Fig. 6b shows the variation of η with the steam-to-methane molar ratios for different ϵ values. The η decreases significantly with the increase in steam-to-methane ratio. This is due to the significant increase in energy required to generate steam for higher ratios. Although an increase in ϵ increases η, but its effect (over η) is not significant. A η of 41% can be achieved for calcination temperature $T_{cal} = 1500$ K, carbonation temperature $T_{carb} = 800$ K, $\epsilon = 0.9$, steam-to-methane ratio $= 4$, and $C = 2000$. Further increase in η can be achieved by recuperating heat from the high-temperature solid products from the calcination reaction (Fig. 6c). Solid heat recovery does not have a huge impact on the process efficiency due to the large amount of heat required for the steam formation to increase the steam-to-methane molar ratio. For 100% solid heat recovery, a η up to 43.5% can be achieved.

These η data, together with data reported by Rubin and Karni [14], Hinkley [42], and Gokon et al. [15] are summarized in Table 1 for comparison. As mentioned earlier, there is no study on CSP-integrated SE-SMR process available in the literature, therefore we could not find the η of this process from other sources to compare. Additionally, although the CSP-integrated SMR processes have been investigated at many place, the η values were often times calculated by different approaches and therefore are not included in the table to avoid unfair assessment. In addition to considering a more efficient SE-SMR process to begin with, our η values are higher than the other studies because of two main reasons. First, the proposed process considers the heat recovery from solids using the counter-flow heat exchangers, which has not been considered before. The proposed two reactors approach, in which solid reactive material can move in between the reactors, provides a counter-flow heat exchange with ~ 90% chance of recovering heat from the solids [43], and thereby improving the total efficiency of the process. Secondly, the proposed process upgrades the heating value of CH_4 because, on a molar basis, H_2 (70.89 MJ mol^{-1}) has much higher heating value in comparison to CO (0.36 MJ mol^{-1}), which is one of the main components of syngas (*i.e.* output of the SMR process) [44]. None of the other studies considers this penalty of energy cost to separate CH_4 and CO_2 from the product gases, which reduces their overall process efficiency. Moreover, a pure CO_2 stream can be obtained from the proposed process during the calcination step. By performing the calcination reaction in 100% CO_2 atmosphere, a pure CO_2 product stream from this reactor is possible, which is suitable for storage or reused. While this reaction condition will increase the calcination temperature, thereby decreasing the overall process efficiency, this can be averted by incorporating a vacuum pump-assisted calcination process. With the reduction in partial pressure of CO_2 during the calcination process, the calcination temperature can be decreased which can both improve the solar-to-fuel efficiency and recover the pure CO_2 stream for further utilization. Further study is needed, however, to assess the overall impact of energy penalty of vacuum pumping operation and the energy gain of reducing the calcination temperature over the final solar-to-fuel efficiency of the proposed process.

Table 1
Limited data of solar-to-fuel efficiency (η) for solar thermal-integrated SMR and SE-SMR processes.

Year	Authors	Type of process (SMR or SE-SMR)	Max.η %
2011	Rubin & Karni [14]	SMR; tested on a solar tower	30[†]
2014	Hinkley[‡] [42]	SMR; tested on a solar tower	34
2014	Gokon et. al [15]	SMR; lab-scale reactor integrated with molten carbonate salts-based thermal energy storage system	29
	Current study ($T_{cal} = 1500$ K, $T_{carb} = 800$ K, $\epsilon = 0.9$, steam-to-methane ratio $= 4$, and $C = 2000$)Refer to Fig. 6c	SE-SMR; analytical study (without solid heat recovery)	41
	Current study ($T_{cal} = 1500$ K, $T_{carb} = 800$ K, $\epsilon = 0.9$, steam-to-methane ratio $= 4$, and $C = 2000$)Refer to Fig. 6c	SE-SMR; analytical study (with solid heat recovery)	43.5

[†] Value is calculated using experimental data taken from Rubin and Karni [14].
[‡] Cited in Yadav et al. [12].

4. Conclusions

The present thermodynamic study considered four metal carbonate/metal oxide pairs ($SrO/SrCO_3$, $MgO/MgCO_3$, $BaO/BaCO_3$, and $CaO/CaCO_3$) in a solar thermal sorption-enhanced steam methane reforming (SE-SMR) process for direct fuel (H_2) production. This study represents the first integration of concentrating solar power (CSP) with the SE-SMR process. The results show that using $CaCO_3/CaO$ pair can enable efficient (up to 43.5%) direct conversion of solar energy to high-quality H_2. For the carbonation reaction, required operating temperatures between 700 and 900 K at 1 bar pressure are suggested by a reactor-scale thermodynamic model. The calcination reaction shows close-to-complete conversion around 1500 K temperature at the pressure of 1 bar. Moreover, the thermodynamic model predicts the necessity of using a higher steam-to-methane ratio to avoid the formation of carbonaceous gases

and unreacted CH_4 in the exhaust stream. The steam-to-methane ratio $\geq$ 4 is recommended for the carbonation reaction. Furthermore, an advanced process model, based on the thermodynamic model, was developed to determine the solar-to-fuel efficiency (η). The model predicts a $\eta \sim 41\%$ for steam-to-methane ratio of 4, without considering any solid phase heat recovery. For a higher steam-to-methane ratio, efficiency decreases because of an increase in energy required to generate higher amounts of steam. The energy balance of the complete process is dominated by the energy required to generate steam due to which only a slight (2.5%) increase in efficiency is predicted by incorporating solid phase heat recovery. Nonetheless, a solar-to-fuel efficiency comparison shows that the proposed solar thermal SE-SMR process can obtain higher efficiency than the solar-assisted SMR processes because it can directly generate H_2, which has a higher heating value than syngas that is generated in SMR. In addition, the innovative two reactors system configuration considered in this study provides an opportunity of having highly efficient (>90%) counter-flow heat exchange for the solid phase heat recovery. Even though moving solid particles between reactors can be practically challenging, it provides an integrated thermochemical heat storage opportunity that mitigates the intermittency impact of solar radiations by decoupling the calcination (endothermic) and carbonation (exothermic) processes. Additionally, the calcination and carbonation reactors can be optimized separately based on their reaction kinetics, making them more efficient and compact. We have not extended our model beyond the four metal carbonate/metal oxide pairs. However, we hope that the simple analytical model such as the one developed and described herein will be useful for future researchers and engineers to build upon and further optimize this solar thermal-driven SE-SMR process beyond the $CaCO_3$/CaO pair.

Data availability

The data that support the findings of this study are available from the corresponding authors upon reasonable request.

Declaration of Competing Interest

The authors declare that they have no known competing financial interests or personal relationships that could have appeared to influence the work reported in this paper.

Acknowledgements

This research did not receive any specific grant from funding agencies in the public, commercial, or not-for-profit sectors.

References

[1] Mazloomi K, Gomes C. Hydrogen as an energy carrier: prospects and challenges. Renew Sustain Energy Rev 2012;16(5):3024–33. https://doi.org/10.1016/j.rser.2012.02.028.

[2] Klausner JF, Li L, Singh A, Yeung NA, Mei R, Hahn D, et al. The role of heat transfer in sunlight to fuel conversion using high temperature solat thermochemical reactors. Proc 15th Int Heat Transf Conf. Kyoto, Japan 2014:221-50. 10.1615/IHTC15.kn.000012.

[3] Edwards RL, Font-Palma C, Howe J. The status of hydrogen technologies in the UK: a multi-disciplinary review. Sustain Energy Technol Assess 2021;43:100901. https://doi.org/10.1016/j.seta.2020.100901.

[4] Harrison DP. Sorption-enhanced hydrogen production: a review. Ind Eng Chem Res 2008;47(17):6486–501. https://doi.org/10.1021/ie800298z.

[5] Shokrollahi Yancheshmeh M, Radfarnia HR, Iliuta MC. High temperature CO_2 sorbents and their application for hydrogen production by sorption enhanced steam reforming process. Chem Eng J 2016;283:420–44. https://doi.org/10.1016/j.cej.2015.06.060.

[6] Di Giuliano A, Gallucci K. Sorption enhanced steam methane reforming based on nickel and calcium looping: a review. Chem Eng Process 2018;130:240–52. https://doi.org/10.1016/j.cep.2018.06.021.

[7] Wang Y, Memon MZ, Seelro MA, Fu W, Gao Y, Dong Y, et al. A review of CO_2 sorbents for promoting hydrogen production in the sorption-enhanced steam reforming process. Int J Hydrogen Energy 2021;46(45):23358–79. https://doi.org/10.1016/j.ijhydene.2021.01.206.

[8] Ji G, Yao JG, Clough PT, da Costa JCD, Anthony EJ, Fennell PS, et al. Enhanced hydrogen production from thermochemical processes. Energy Environ Sci 2018;11(10):2647–72.

[9] Gunawan A, Simmons RA, Haynes MW, Moreno D, Menon AK, Hatzell MC, et al. Techno-economics of cogeneration approaches for combined power and desalination from concentrated solar power. J Sol Energy Eng 2019;141(2). https://doi.org/10.1115/1.4042061.

[10] Gunawan A, Singh AK, Simmons RA, Haynes MW, Limia A, Ha JM, et al. A cost-performance analysis of a sodium heat engine for distributed concentrating solar power. Adv Sustain Syst 2020;4(6):1900104. https://doi.org/10.1002/adsu.201900104.

[11] Agrafiotis C, von Storch H, Roeb M, Sattler C. Solar thermal reforming of methane feedstocks for hydrogen and syngas production-a review. Renew Sustain Energy Rev 2014;29:656–82. https://doi.org/10.1016/j.rser.2013.08.050.

[12] Yadav D, Banerjee R. A review of solar thermochemical processes. Renew Sustain Energy Rev 2016;54:497–532. https://doi.org/10.1016/j.rser.2015.10.026.

[13] Meloni E, Martino M, Palma V. A short review on Ni based catalysts and related engineering issues for methane steam reforming. Catalysts 2020;10(3):352. https://doi.org/10.3390/catal10030352.

[14] Rubin R, Karni J. Carbon dioxide reforming of methane in directly irradiated solar reactor with porcupine absorber. J Sol Energy Eng 2011;133. https://doi.org/10.1115/1.4003678.

[15] Gokon N, Nakamura S, Hatamachi T, Kodama T. Steam reforming of methane using double-walled reformer tubes containing high-temperature thermal storage Na_2CO_3/MgO composites for solar fuel production. Energy 2014;68:773–82. https://doi.org/10.1016/j.energy.2014.01.107.

[16] Pashchenko D. Experimental investigation of reforming and flow characteristics of a steam methane reformer filled with nickel catalyst of various shapes. Energy Convers Manage 2019;185:465–72. https://doi.org/10.1016/j.enconman.2019.01.103.

[17] Giaconia A, Iaquaniello G, Caputo G, Morico B, Salladini A, Turchetti L, et al. Experimental validation of a pilot membrane reactor for hydrogen production by solar steam reforming of methane at maximum 550 °C using molten salts as heat transfer fluid. Int J Hydrogen Energy 2020;45(58):33088–101. https://doi.org/10.1016/j.ijhydene.2020.09.070.

[18] Bulfin B, Ackermann S, Furler P, Steinfeld A. Thermodynamic comparison of solar methane reforming via catalytic and redox cycle routes. Sol Energy 2021;215:169–78. https://doi.org/10.1016/j.solener.2020.11.076.

[19] Koumi Ngoh S, Ayina Ohandja LM, Kemajou A, Monkam L. Design and simulation of hybrid solar high-temperature hydrogen production system using both solar photovoltaic and thermal energy. Sustain Energy Technol Assess 2014;7:279–93. https://doi.org/10.1016/j.seta.2014.05.002.

[20] Said SAM, Simakov DSA, Waseeuddin M, Roman-Leshkov Y. Solar molten salt heated membrane reformer for natural gas upgrading and hydrogen generation: a CFD model. Sol Energy 2016;124:163–76. https://doi.org/10.1016/j.solener.2015.11.038.

[21] Wang HS, Liu MK, Kong H, Hao Y. Thermodynamic analysis on mid/low temperature solar methane steam reforming with hydrogen permeation membrane reactors. Appl Therm Eng 2019;152:925–36. https://doi.org/10.1016/j.applthermaleng.2018.03.030.

[22] Pashchenko D. Thermodynamic equilibrium analysis of steam methane reforming based on a conjugate solution of material balance and law action mass equations with the detailed energy balance. Int J Energy Res 2020;44(1):438–47. https://doi.org/10.1002/er.4943.

[23] Di Felice L, Kazi SS, Sørby MH, Martinez I, Grasa G, Maury D, et al. Combined sorbent and catalyst material for sorption enhanced reforming of methane under cyclic regeneration in presence of H_2O and CO_2. Fuel Process Technol 2019;183:35–47. https://doi.org/10.1016/j.fuproc.2018.10.012.

[24] Di Giuliano A, Gallucci K, Di Carlo A, Stendardo S, Courson C, Foscolo PU. Sorption enhanced steam methane reforming by Ni/CaO/mayenite combined systems: overview of experimental results from European research project ASCENT. Can J Chem Eng 2020;98:1907–23. https://doi.org/10.1002/cjce.23779.

[25] Acha E, Chen D, Cambra JF. Comparison of novel olivine supported catalysts for high purity hydrogen production by CO_2 sorption enhanced steam reforming. J CO_2 Util 2020;42:101295. https://doi.org/10.1016/j.jcou.2020.101295.

[26] Chen C-H, Yu C-T, Chen W-H. Improvement of steam methane reforming via in-situ CO_2 sorption over a nickel-calcium composite catalyst. Int J Hydrogen Energy 2021;46(31):16655–66. https://doi.org/10.1016/j.ijhydene.2020.08.284.

[27] Phuakpunk K, Chalermsinsuwan B, Putivisutisak S, Assabumrungrat S. Simulations of sorbent regeneration in a circulating fluidized bed system for sorption enhanced steam reforming with dolomite. Particuology 2020;50:156–72. https://doi.org/10.1016/j.partic.2019.08.005.

[28] Nkulikiyinka P, Yan Y, Güleç F, Manovic V, Clough PT. Prediction of sorption enhanced steam methane reforming products from machine learning based soft-sensor models. Energy and AI 2020;2:100037. https://doi.org/10.1016/j.egyai.2020.100037.

[29] Yan Y, Thanganadar D, Clough PT, Mukherjee S, Patchigolla K, Manovic V, et al. Process simulations of blue hydrogen production by upgraded sorption enhanced steam methane reforming (SE-SMR) processes. Energy Convers Manage 2020;222:113144. https://doi.org/10.1016/j.enconman.2020.113144.

[30] Neni A, Benguerba Y, Balsamo M, Erto A, Ernst B, Benachour D. Numerical study of sorption-enhanced methane steam reforming over Ni/Al_2O_3 catalyst in a fixed-bed reactor. Int J Heat Mass Transfer 2021;165:120635. https://doi.org/10.1016/j.ijheatmasstransfer.2020.120635.

[31] Ermanoski I, Grobbel J, Singh A, Lapp J, Brendelberger S, Roeb M, et al. Design and construction of a cascading pressure reactor prototype for solar-thermochemical

hydrogen production. AIP Conf Proc 2016;1734:120001. https://doi.org/10.1063/1.4949203.
[32] Lackner KS. Climate change. A guide to CO_2 sequestration. Science 2003;300 (5626):1677–8.
[33] Centi G, Perathoner S. Perspectives and state of the art in producing solar fuels and chemicals from CO_2. In: Centi G, Perathoner S, editors. Green carbon dioxide: Advances in CO_2 utilization. New York: John Wiley & Sons, Inc.; 2014. p. 1–24.
[34] Singh A, Al-Raqom F, Klausner J, Petrasch J. Production of hydrogen via an iron/iron oxide looping cycle: thermodynamic modeling and experimental validation. Int J Hydrogen Energy 2012;37(9):7442–50. https://doi.org/10.1016/j.ijhydene.2012.01.074.
[35] Bale CW, Bélisle E, Chartrand P, Decterov SA, Eriksson G, Gheribi AE, et al. Factsage thermochemical software and databases, 2010–2016. Calphad 2016;54:35–53. https://doi.org/10.1016/j.calphad.2016.05.002.
[36] Krenzke PT, Davidson JH. Thermodynamic analysis of syngas production via the solar thermochemical cerium oxide redox cycle with methane-driven reduction. Energy Fuels 2014;28:4088–95. https://doi.org/10.1021/ef500610n.
[37] Lapp J, Davidson JH, Lipinski W. Efficiency of two-step solar thermochemical non-stoichiometric redox cycles with heat recovery. Energy 2012;37:591–600. https://doi.org/10.1016/j.energy.2011.10.045.
[38] Singh AK, AuYeung NJ, Randhir K, Mishra R, Allen KM, Petrasch J, et al. Thermal reduction of iron oxide under reduced pressure and implications on thermal conversion efficiency for solar thermochemical fuel production. Ind Eng Chem Res 2015;54:6793–803. https://doi.org/10.1021/ie504402x.
[39] Broda M, Manovic V, Imtiaz Q, Kierzkowska AM, Anthony EJ, Muller CR. High-purity hydrogen via the sorption-enhanced steam methane reforming reaction over a synthetic CaO-based sorbent and a Ni catalyst. Environ Sci Technol 2013;47:6007–14. https://doi.org/10.1021/es305113p.
[40] Chanburanasiri N, Ribeiro AM, Rodrigues AE, Arpornwichanop A, Laosiripojana N, Praserthdam P, et al. Hydrogen production via sorption enhanced steam methane reforming process using Ni/CaO multifunctional catalyst. Ind Eng Chem Res 2011;50:13662–71. https://doi.org/10.1021/ie201226j.
[41] Singh A. Thermodynamic analysis of syngas production and sulfur capturing from a mixture of methane and hydrogen sulfide using a solar thermochemical redox cycle. Ind Eng Chem Res 2018;57:11738–46. https://doi.org/10.1021/acs.iecr.8b02484.
[42] Hinkley J. Solar fuels research at CSIRO (presentation at the international workshop of design of sub-systems for concentrated solar power technologies, 19-22 December 2013), http://www.iitj.ac.in/CSP/material/20dec/fuels.pdf; 2013 [accessed 11 July 2020].
[43] Holzemer-Zerhusen P, Brendelberger S, Roeb M, Sattler C. Oxygen crossover in solid-solid heat exchangers for solar water and carbon dioxide splitting: A thermodynamic analysis. Proc ASME 2020 14th Int Conf on Energy Sustain. Virtual, Online 2020;V001T13A001. 10.1115/es2020-1608.
[44] Lee MC, Seo SB, Chung JH, Kim SM, Joo YJ, Ahn DH. Gas turbine combustion performance test of hydrogen and carbon monoxide synthetic gas. Fuel 2010;89:1485–91. https://doi.org/10.1016/j.fuel.2009.10.004.